An eco-friendly and cleaner process for preparing architectural ceramics from coal fly ash: Pre-activation of coal fly ash by a mechanochemical method

Yang Luo [a, b, c], Ying-hong Wu [a, b, d], Shu-hua Ma [a], Shi-li Zheng [a, *], Paul K. Chu [c, **]

[a] National Engineering Laboratory for Hydrometallurgical Cleaner Production Technology, CAS Key Laboratory of Green Process and Engineering, Institute of Process Engineering, Chinese Academy of Sciences, Beijing, 100190, China
[b] University of Chinese Academy of Sciences, Beijing, 100049, China
[c] Department of Physics and Department of Materials Science and Engineering, City University of Hong Kong, Tat Chee Avenue, Kowloon, Hong Kong, China
[d] School of Energy and Environment, City University of Hong Kong, Tat Chee Avenue, Kowloon, Hong Kong, China

ARTICLE INFO

ABSTRACT

Using coal fly ash (CFA) as the raw materials in ceramic production is an effective means to realize large-quantity and high-value utilization. An eco-friendly and cleaner process to prepare architectural ceramics from CFA is described in this paper. CFA first undergoes mechanochemical activation and then used to prepare porcelain ceramic tiles with outstanding mechanical properties. The solution after activation is the sole raw materials to produce foamed ceramics with novel thermal insulation properties. The mechanochemical activation mechanism is investigated systematically. During activation, some of the octahedrally coordinated Al^{3+} ions are converted into tetrahedrally coordinated Al^{3+}, which can substitute for Si^{4+} in the tetrahedral rendering the silicate structure in activated CFA unstable. Moreover, the preparation mechanism of the foamed ceramics is studied. On the micro-level, solidification of the foamed ceramics can be interpreted as Si-O-Si structural transformation from two-dimensional layers to a three-dimensional network during sintering. The two final products are characterized and the good mechanical properties of as-obtained porcelain ceramic tiles are attributed to the needle-shape mullite derived from activated CFA. The low thermal conductivity of 0.0453 W/m·K of the as-obtained foamed ceramics arises from the unique cavity construction. Finally, the substance flow, gas emission, and heavy metal leaching behavior of the final products are discussed and the results indicate that there is almost no hazardous waste emission in the process. This study provides insights into more efficient and cleaner utilization of CFA as ceramic materials.

© 2019 Elsevier Ltd. All rights reserved.

1. Introduction

Coal fly ash (CFA) is a type of solid waste residue produced in coal-fired power plants. With the rapid development of the electric power industry in China, the discharge of CFA has increased year by year (Wang et al., 2016). According to statistics, China's discharge of CFA in 2015 reaches 620 million tons, and the annual generation is still increasing (Sun et al., 2017). Although the utilization rate of CFA in China has reached 70%, there are still a large number of CFA deposits due to the huge discharge and it is causing serious environmental pollution problems (Ma et al., 2018). CFA is used mainly in China in road pavements (Li et al., 2018a), mine backfills (Park et al., 2014), and soil amelioration (Yao et al., 2015) but the traditional utilization schemes are "low-tech" and do not add much value. Therefore, it is urgent to develop a new technology that can consume large amounts of CFA and simultaneously produce high value-adding products.

Rapid urbanization of China in the past two decades has led to rapid development of the ceramics industry. China produced 10.23

billion square meters of ceramic tiles in 2015, which ranked first in the world (Wang et al., 2018). However, expansion of ceramic production leads to shortage of raw materials and it is important for the industry to find new alternative raw materials and new production technology (Huang et al., 2013). CFA is an aluminosilicate similar to finished porcelain ceramic tiles with regard to the chemical and phase composition. Hence, using CFA as a substitute as traditional porcelain ceramic raw materials has large industrial potential.

The raw materials of porcelain ceramic tiles usually include quartz (5—30 wt%), feldspar (20—40 wt%) and clay (30—55 wt%) (Carty and Senapati, 1998; Kamseu et al., 2007). In the mixture, quartz is quite stable during sintering and so it acts as an inert filler to decrease the deformation and shrinkage of the ceramics (Reinosa et al., 2015). Feldspar as a fluxing agent promote densification to produce a dense matrix (Wattanasiriwech and Wattanasiriwech, 2011) and clay serves as a binder for the other constituents in the green body to provide the required plasticity for molding (Turkmen et al., 2015). A more important function of clay is to form mullite crystals during sintering to provide strength in the porcelain ceramic tiles (Leonelli et al., 2001). CFA can be used to substitute raw materials with high environmental benefits (Bontempi, 2017). Currently, CFA is used to substitute for quartz because CFA particles are relatively inert in the sintering process. Gradual substitution of CFA for quartz has been studied by increasing the CFA content from 5 wt% to 15 wt% (Dana et al., 2004). The substitution increases the linear shrinkage and bulk density and decreases the apparent porosity in the entire temperature range of 1150—1300 °C. Mukhopadhyay et al. (2010) used CFA to substitute for quartz in a traditional triaxial porcelain composition and the specimen with 30 wt% CFA showed approximately 20% increase in the flexural strength compared to the conventional triaxial body. In another study by Pal and Das (2018), complete substitution of quartz by CFA in the porcelain body with 15% CFA reduced the vitrification temperature and enhanced the strength of the body. When CFA is rich in alkali and alkaline earth elements, it can substitute some feldspar to accelerate melting. In the study conducted by Olgun et al. (2005), the wall tiles were produced by replacing potassium feldspar with Turkish CFA in the range of 2—10 wt%. The firing strength of the tile increased when a moderate amount of CFA was used to prepare the standard tile composition. However, an excess amount of fluxing components (Na, K, Si) decreased the strength when the CFA content was 10 wt%. Two different types of fly ash were used to substitute for the feldspar in porcelain ceramics (Kockal, 2012). The alkali metals (Na, K) in CFA were beneficial to melt viscosity reduction and ceramic densification, while abundant alkaline earth metals (Ca, Mg) caused a sharp drop in the melt viscosity and deteriorated the performance. Currently, the amount of CFA incorporated into ceramic materials is always less than 50 wt% because the present technology can only use fly ash to substitute for quartz and a small amount of feldspar (Das et al., 2013). CFA was substituted for clay in ceramic formulations of porcelain, but the substitution effect was not ideal. Kumar et al. (2001) gradually replaced the clay component in porcelain ceramic materials by CFA and investigated the substitution effects on the production process and product performance. When CFA addition exceeded 25 wt%, the content of mullite crystals decreased sharply along with an increase in the glass content, causing large performance deterioration. If CFA can substitute some clay to form excellent secondary mullite crystals, the amount of added CFA may increase significantly.

Buildings are responsible for approximately 40% of the world global energy consumption (Novais et al., 2016). The energy demand has been increasing at a rate of 1.8% per year over the last 40 years and to nearly 58% by 2050 (Allouhi et al., 2015). Hence, architectural thermal insulation materials are necessary to reduce building energy consumption and limit global greenhouse gas emission. However, the common organic thermal insulation materials are flammable (Kairytė et al., 2018; Li et al., 2015) and increasing attention has been paid to inorganic thermal insulation materials. For example, foamed ceramics is one of the most potent architectural thermal insulation materials due to the good fireproofing properties, high mechanical strength, thermal insulation, sound insulation, and moisture resistance (Han et al., 2017; König et al., 2015). The current foamed ceramics are mainly prepared by adding a foaming agent to produce the desirable porosity. Nevertheless, owing to the poor dispersion of foaming agents in the system, the low thermal conductivity is obtained at the expense of low compressive strength, or high compressive strength is obtained at the expense of high thermal conductivity (Luo et al., 2018). For example, Cao et al. (2015) prepared a highly porous ceramic foam (from fly ash) with a low thermal conductivity of 0.0590 W/(m·K), but the concomitant compressive strength was only 0.31 MPa. Zhu et al. (2016) prepared ceramic foams (using coal fly ash and waste glass) with a considerable compressive strength of 5 MPa, but the foams have relatively high thermal conductivity of 0.36 W/m·K. Therefore, a novel type of foamed ceramics with good thermal insulation properties and mechanical properties is important to the industry.

In our previous study, an alkali activation pretreatment of CFA was designed to improve the properties of CFA as ceramic materials (Luo et al., 2017). After alkali activation, the amount of added CFA and the properties of the porcelain ceramic tiles were enhanced significantly. However, the long high-pressure hydrothermal activation conditions adversely affected the production efficiency and the discharged alkaline solution with a small SiO2 concentration made it difficult for ceramic manufacturers to utilize. The aim of this study is to design a more practical utilization technique for CFA in architectural ceramics production without hazardous waste emission. Herein, efficient mechanochemical activation is implemented to pre-process CFA. The activated CFA serves as the main raw materials to prepare porcelain ceramic tiles with good mechanical properties and the solution after activation is the sole raw material to produce foamed ceramics with novel thermal insulation properties. The mechanism pertaining to mechanochemical activation and preparation mechanism of the foamed ceramics are discussed. The two final products are characterized and issues related to substance flow, gas emission, and heavy metal leaching are discussed.

1.1. Materials

The CFA used in this experiment is a kind of wet discharged ash, generated by combustion of typical lignite obtained from the pulverized coal boiler of a thermoelectric power plant in Inner Mongolia, China. The untreated CFA was inert during sintering and played a quartz-like role in the ceramics (Luo et al., 2017). Sodium hydroxide (NaOH) and hydrofluoric acid (HF, 40.0 wt%) were reagent grade (Xilong Chemical Co., Ltd., China) and used as received without further purification. The feldspar and high plastic clay obtained from a ceramics manufacturer in Shandong, China were used as the ceramic ingredients. The chemical composition is shown in Table 1 and the ICP-OES measurement is described in Section 2.3.

Table 1
Chemical composition of feldspar and kaolin (wt%) measured by ICP-OES.

Sample	Al_2O_3	SiO_2	Fe_2O_3	TiO_2	CaO	MgO	Na_2O	K_2O	LOI
Feldspar	20.57	66.98	0.10	0.06	0.05	0.00	11.66	0.03	0.55
High plastic clay	26.58	68.74	0.40	0.03	0.47	0.52	0.36	1.21	1.77

LOI: Loss on ignition.

1.2. Experimental procedures

The schematic diagram of the process is shown in Fig. 1. The key to the whole process is coupled mechanochemical activation of CFA in the NaOH solution and there are two routes. The first was to prepare porcelain ceramic tiles from the activated CFA solid and the second was to prepare foamed ceramics from the solution after activation. The processing parameters were optimized by considering the technical and economical feasibility.

Mechanochemical activation of CFA was conducted in a 1-L planetary ball mill (Model PULVERISETTE 6, FRITSCH Scientific Instruments Co., Ltd., Germany). CFA and 10.0 wt% NaOH were added to the reactor at a liquid-to-solid ratio of 2.5 mL/g, and the mixture was milled at a speed of 400 rpm for 2 h. After activation, the slurry was filtered to separate the activated CFA and solution. The activated CFA was washed five times with hot deionized water (95 °C) and dried in an oven at 105 °C for 12 h prior to the analysis and preparation of the porcelain ceramic tiles.

The porcelain ceramic tiles were prepared by a conventional ceramic production method. Prior to making the green compact, ~55 wt% activated CFA was homogenized by milling with ~35 wt% feldspar and ~10 wt% high plastic clay. In preparing the green compact, the homogeneous raw materials were mixed with deionized water with a 10:2 mass ratio and the mixture was pressed into 10 cm × 10 cm × 0.5 cm cuboids using a uniaxial tablet press (Model 769 YP-60E, Tianjin Keqi High & New Technology Corporation, China). The green compacts were dried at 105 °C for 12 h. In the subsequent sintering stage, the green compacts were heated from room temperature to 1100 °C at a rate of 5 °C/min, held for 1 h, and cooled to room temperature at the rate of 3 °C/min in a laboratory electrical sintering furnace (Model SX-G13135, Tianjin Zhonghuan Lab Furnace Co., Ltd, China). A reference sample was prepared under the same conditions in addition to replacing activated CFA with untreated CFA. Production of foamed ceramic samples from alkali-activated CFA involved pouring the solution after activation into cylindrical molds with a diameter of 70 mm and height of 100 mm and sintering in the laboratory electrical sintering furnace at 600 °C for 30 min at a heating rate of 5 °C/min and cooling rate of 3 °C/min.

1.3. Characterization

An inductively-coupled plasma optical emission spectrometer (ICP-OES Model Optima 7300 V, PerkinElmer Inc., USA) was used to determine the chemical composition of the samples. Before the analysis, a pre-digestion method was adopted and the detailed operation is described in the Supplementary Material. The
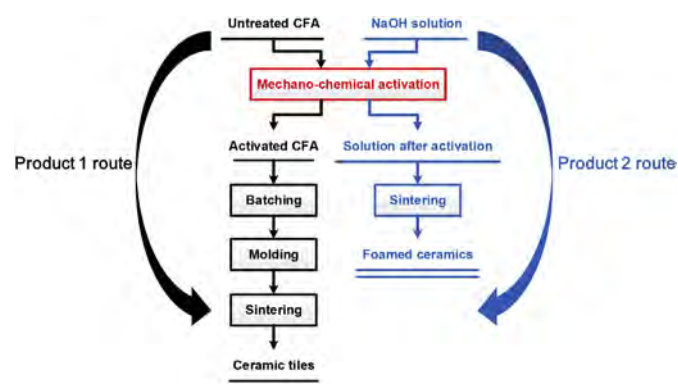
solutions obtained from the heavy metal leaching test were analyzed by inductively-coupled plasma-mass spectrometry (ICP-MS, Model iCAP Qc, Thermo Scientific, USA). The phase of the solid samples was identified by X-ray diffraction (XRD, Model X'pert Pro MPD, PANalytical B.V., Netherlands) with Cu K_α radiation at 40 kV and 30 mA. The morphological and mineralogical analyses were conducted on a scanning electron microscope (SEM, Model JSM-7100F, JEOL Co., Ltd., Japan) at 25 kV and the sample composition was determined by energy-dispersive X-ray spectroscopy (EDS). The particle size distribution was determined on a particle-size analyzer (Model Mastersizer, 2000; Malvern Panalytical Ltd., UK). The solid-state ^{29}Si magic angle spinning nuclear magnetic resonance spectra (MAS-NMR, Model AVANCE III HD 400 MHz, Bruker Corporation, Switzerland) were acquired at 9.4 MHz using a 4-mm MAS probe at spinning speed of 8.0 kHz. The ^{27}Al MAS NMR spectra were acquired at 104.0 MHz at a spinning speed of 12.0 kHz. High-power decoupling was used and the ^{29}Si spectra were recorded for a 5-s recycle time and a 45° pulse width of 2 μs. The ^{27}Al spectra were obtained using a 1-s recycle time and a 30° pulse width of 1 μs. The solution after activation was analyzed by thermogravimetric analysis and differential scanning calorimetry (TG-DSC, Model NETZSCH STA 449 C, Germany) in air at a heating rate of 20 °C/min. Fourier transform infrared spectroscopy (FTIR, Model 100FT-IR, PerkinElmer Inc., USA) were performed in the wavenumber range from 4000 to 400 cm^{-1} with 2 cm^{-1} spectral resolution. During the FTIR measurement, 2 mg of each type of materials after drying were mixed with KBr with spectroscopic purity at a mass ratio of 1:100 and the mixture was pressed into a round pellet at 30 MPa using a manually operated hydraulic press. The structure of the porous structure inside the as-obtained foamed ceramic sample were observed by 3D X-ray tomography (Model Zeiss Xradia 410 Versa, Carl Zeiss AG, USA). A cylindrical sample with a diameter and height of 3 mm was scanned with a polychromatic beam with energy up to 50 kV and the 3D density map was reconstructed by standard filtered back projection during 360° sample rotation.

The apparent density of the ceramic samples was calculated from the mass-to-volume ratio and the water absorption and open porosity of the porcelain ceramic tile samples were determined by the Archimedes method according to ASTM C373. The thermal shock behavior of porcelain ceramic tile samples was assessed by bearing times (without obvious cracks) according to a rapid quenching method. The samples were heated to 1100 °C and held for 5 min, followed by rapid cooling for 5 min (on the surface of iron partly submerged in water at 25 °C). The porosity of the foamed ceramic samples was calculated from the apparent density and powder true density using the equation: porosity (%) = (1 − apparent density/powder true density) × 100. The true density was determined with ground ceramic powders by the pycnometry method according to the Chinese standard GB/T 5071−2013. The thermal conductivity of the foamed ceramic samples at 25 °C was measured on a transient hot-wire thermoconductivity tester (Model TC 3000E, Xi'an Xiatech Electronics Co., Ltd., China). The rupture modulus of the porcelain ceramic tile samples and compressive strength of foamed ceramic samples were determined on an electronic universal testing machine (Model WDW-20E, Jinan Shidai Shijin Testing Machine Group Co., Ltd., China). The reported values were averages of five replicate measurements.

The obtained ceramic samples were crushed and the resultant granules with a particle size between 1 mm and 3 mm were used to assess the heavy metal leaching behavior according to GB 5086.2−1997 (Chinese standard of solid waste—extraction procedure for toxicity of solid waste—horizontal vibration method). The one-stage batch leaching test was performed as follows conditions. The leachant was ultrapure water, liquid-to-solid ratio was

Fig. 1. Flow diagram of the process.

10 mL/g, horizontal oscillation frequency was 110 time/min, oscillation amplitude was 40 mm, oscillation temperature was 25 °C; oscillation time was 8 h, and standing time was 18 h. The heavy metal standard limits were defined according to GB 5085.3–2007 (Chinese identification standard of hazardous waste-—identification of leaching toxicity).

2. Results and discussion

2.1. Mechanism of mechanochemical activation

To study the activation effects, a detailed comparison of the untreated CFA and activated CFA is carried out using SEM, XRD, particle size analysis, chemical composition analysis, and MAS NMR.

The SEM image in Fig. 2(a) indicates that the untreated CFA are microspheres with a smooth surface. In contrast, irregular fragments with a rough surface are dominant in the activated CFA, as shown in Fig. 2(b). The particle size decreases in the activation process as confirmed by the particle size distributions in Fig. 2(c). The diameter parameter, d (0.5), is the most important indicator in determining the particle size and d (0.5) = N μm means that the size of 50% of the particles is less than or equal to N μm. Fig. 2(c) indicates that d (0.5) is reduced from 37.10 μm of the untreated CFA to 4.05 μm of the activated CFA. The mechanical activation results with regard to particle refinement, surface roughening and energy storage effect provide the pre-condition for coupled chemical activation. The XRD patterns of these two samples in Fig. 2(d) demonstrate that the mineral phases (comprising quartz, mullite, and amorphous phase) do not change in activation but the quartz and amorphous phases decline significantly. The mineral phase change is chiefly attributed to the chemical activation effect. The chemical compositions of the untreated CFA and activated CFA are displayed in Table 1. The SiO_2 content decreases significantly from 58.91 wt% to 19.33 wt% after activation consistent with the amount of reduction of the quartz and amorphous phases revealed by XRD.

84.65% of SiO_2 in CFA dissolves in the liquid phase. The absolute content of Na_2O increases by 1.55%, whereas the absolute contents of the other components barely change during mechanochemical activation. The content increase except Na_2O is concomitant with the decrease in the SiO_2 content. A larger amount of Na_2O is bound to the activated CFA since the solid product is washed thoroughly. Obviously, the synergy of the mechanical and chemical forces leads to the high dissolution rate of SiO_2. The SiO_2 dissolution reaction is represented by Reaction (1):

$$SiO_2 \text{ (s)} + 2 NaOH \text{ (aq)} \rightarrow Na_2SiO_3 \text{ (aq)} + H_2O \text{ (l)} \qquad (1)$$
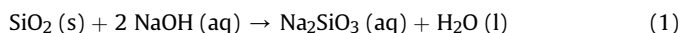
Analysis of the ^{27}Al and ^{29}Si MAS NMR spectra provides understanding aboutf mechanochemical activation on the microscale. The ^{27}Al MAS NMR spectra of the two samples are shown in Fig. 3. The tetrahedrally coordinated Al^{3+} [Al (IV)] resonates at 43 ppm and the octahedrally coordinated Al^{3+} [Al (VI)] resonates at −5 ppm, consistent with previous ^{27}Al MAS NMR studies (Dĕdeček et al., 2009; Oh et al., 2015; Sun et al., 2006). The untreated CFA has an Al (VI)-dominated shape, whereas the activated CFA possesses an Al (IV)-dominated spectrum shape. By calculation, 28.05% of Al (VI) is converted into Al (IV) in the activation process. The peak width of Al (IV) is broader than that of Al (VI). According to the literature (Liu et al., 2013), the Al (VI) usually exists outside the silicate network while the Al (IV) can substitute for Si^{4+} in the tetrahedral network. When Al^{3+} enters the silicate network structure, each Al^{3+} is surrounded by a different environment. The decrease environmental symmetry is conducive to the widening of the Al (IV) peak (Gao et al., 2017; Klinowski et al., 1983). Hence, it can be inferred that a considerable amount of Al (IV) exists in the form of aluminum-oxygen tetrahedra that substitute for silicon-oxygen tetrahedra in the activated CFA.

According to the ^{29}Si MAS NMR spectra (Fig. 4), the variation in the silicate three-dimensional network can be discerned. The silicon-oxygen tetrahedron is usually designated Q^n (mAl), where Q represents a Si atom, n is the number of siloxane bonds attached to
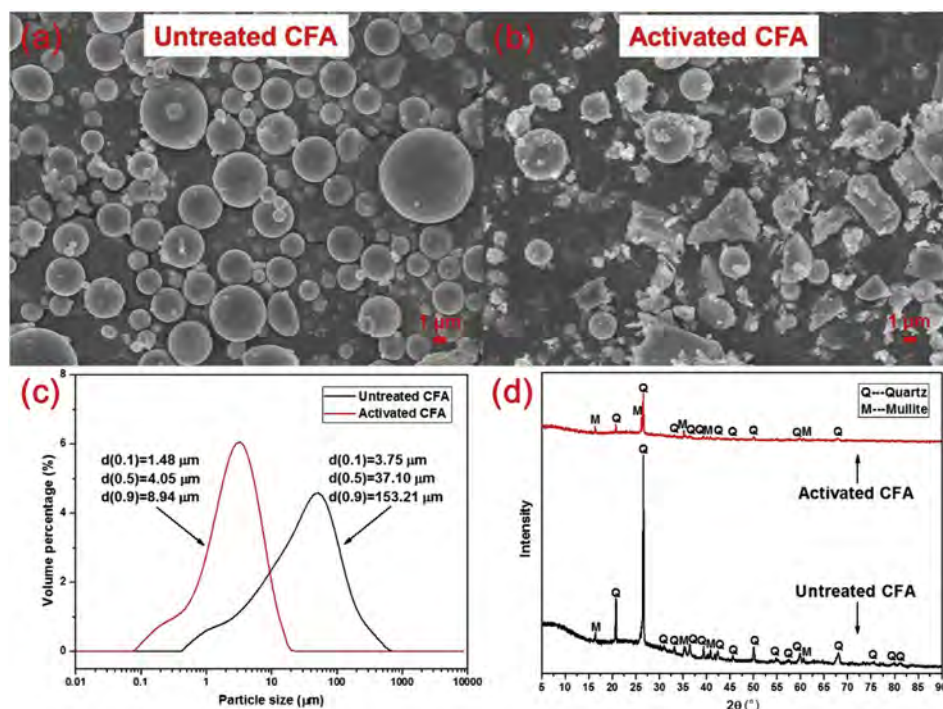

Fig. 2. Characterization of the untreated CFA and activated CFA: (a, b) SEM images, (c) Particle size distributions, and (d) XRD patterns.
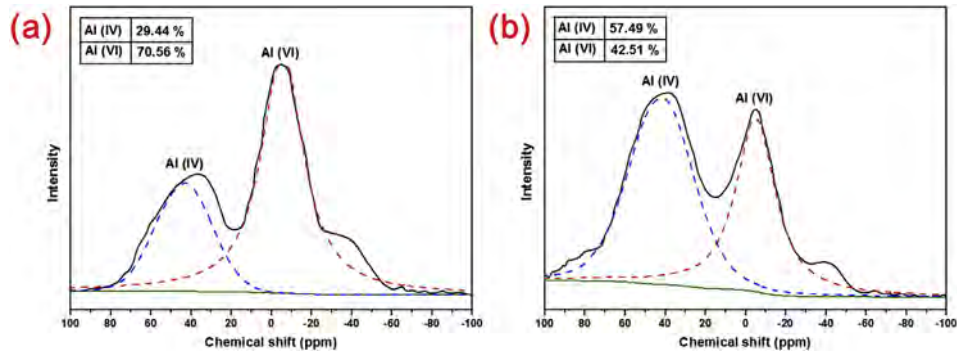
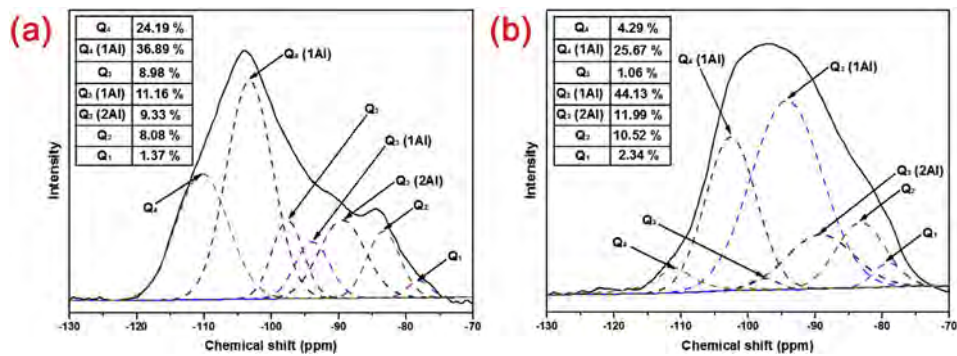**Fig. 3.** ^{27}Al MAS NMR spectra of (a) Untreated CFA and (b) Activated CFA.

Fig. 4. ^{29}Si MAS NMR spectra of (a) Untreated CFA and (b) Activated CFA.

it, and m is the substitution number of adjacent Si^{4+} with Al^{3+}. By deconvoluting the ^{29}Si NMR spectra, the resonance peaks of Q^4, Q^4 (1Al), Q^3, Q^3 (1Al), Q^3 (2Al), Q^2, and Q^1 can be identified at 111 ppm, 103 ppm, 98 ppm, 94 ppm, 89 ppm, 83 ppm, and 79 ppm, respectively (Fernández-Jiménez et al., 2006; He et al., 2004; Oh et al., 2014; Wons et al., 2018). Some subtle changes are related to the relative proportion of various silicon-oxygen tetrahedra in the activation process. The proportion of Q^4, Q^4 (1Al), and Q^3 decreases but the proportion of Q^3 (1Al), Q^3 (2Al), Q^2, and Q^1 increases accordingly, indicating depolymerization of the silicate three-dimensional network. For example, the proportion of Q^4 decreases from 24.19% to 4.29%, while the proportion of Q^3 (1Al) increases from 11.16% to 44.13%. Furthermore, combined with the above ^{27}Al MAS NMR analysis, the dramatic rise of Q^3 (1Al) and Q^3 (2Al) can be ascribed to substitution of Si^{4+} with Al^{3+} [Al (IV)]. Due to the bond length, bond angle and binding energy differences between the aluminum-oxygen tetrahedron and silicon-oxygen tetrahedron, the silicate three-dimensional network of activated CFA is more unstable than that of the untreated CFA (Loewenstein, 1954; Zheng et al., 2012). Therefore, the activated CFA is expected to be more reactive in the subsequent sintering process. Finally, the absolute content increase of Na_2O can be explained. The charge deficit from replacement of Si^{4+} by Al^{3+} in the tetrahedral network of the activated CFA needs to be balanced by adsorption or binding of Na ions (Shi et al., 2013; Sun et al., 2006).

2.2. Preparation mechanism for foamed ceramics

To make better use of the solution after activation, the chemical composition of the solution is determined and the results are shown in Table 3. The solution is composed of mainly Na_2O and SiO_2 together with a tiny amount of Al_2O_3. The modulus (molar

ratio of SiO_2 and Na_2O) of the solution is calculated to be 2.66. The large concentration of SiO_2 in the liquid phase comes from extensive dissolution of the SiO_2 component in CFA in the activation process. The small amount of Al_2O_3 in the solution arises from slight simultaneous dissolution of Al_2O_3. The solution is thought to be a high-modulus sodium silicoaluminate water glass.

TG-DSC analysis of the solution after activation is helpful to condition control and mechanism investigation and the results are displayed in Fig. 5. The TG curve shows that the mass of the solution drops by approximately 76% as the temperature increases from room temperature to 200 °C and then remains unchanged at a higher temperature indicating that water volatilization is completed by 200 °C. The volatile quantity matches the solution composition data in Table 3 quite well. The DSC curve reveals two obvious endothermic peaks at 92 °C and 142 °C. The endothermic peak at 92 °C can be explained by evaporation of a large amount of

Table 2
Chemical composition of untreated CFA and activated CFA (wt%) determined by ICP-OES.

Sample	Al_2O_3	SiO_2	Fe_2O_3	TiO_2	CaO	MgO	Na_2O	K_2O	LOI
Untreated CFA	21.23	58.91	4.49	1.24	6.44	2.73	1.94	1.70	1.32
Activated CFA	38.13	19.33	8.96	2.64	12.92	4.78	4.21	2.57	6.46

LOI: Loss on ignition.

Table 3
Chemical composition of solution after activation (wt%) determined by ICP-OES.

Na_2O	SiO_2	Al_2O_3	H_2O	Modulus
6.44	16.63	1.14	~75.79	2.66

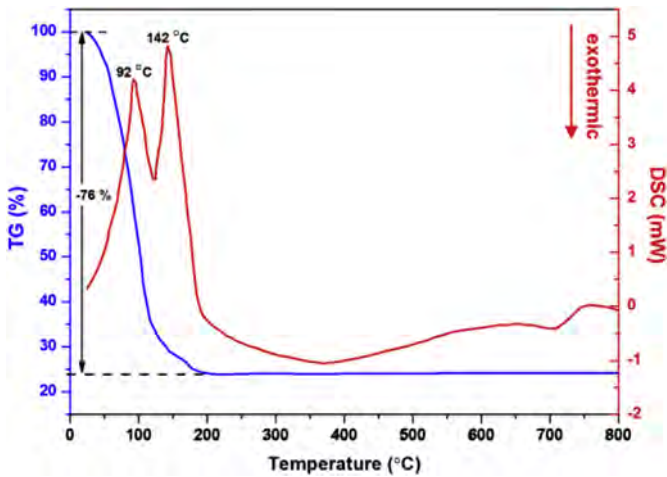Modulus: molar ratio of SiO_2 and Na_2O.

Fig. 5. TG-DSC analysis of the solution after activation.

unbound water and that at 142 °C is ascribed to dehydroxylation of the Si-OH structure since it is accompanied by less mass loss in the TG curve. A broad exothermic valley is observed at 200–600 °C, and this may be caused by condensation polymerization of the precursor structure of the foamed ceramics.

FTIR and ^{29}Si MAS NMR are used to monitor the microstructure change during sintering of the high-modulus water glass. Fig. 6 shows the FTIR spectra of the samples prepared at different temperature. The absorption peaks at 3500 cm^{-1} and 1660 cm^{-1} correspond to the stretching and bending vibrations of the −OH groups, respectively (Rao et al., 2007). Since these two peaks are derived from physically bound waters, the intensity is supposed to decrease significantly when the sample is sintered up to 200 °C. The remaining peaks above 200 °C should be due to a small number of Si−OH groups with good stability. The absorption peaks at 1050 cm^{-1}, 773 cm^{-1} and 450 cm^{-1} are ascribed to the stretching and bending vibrations of the Si−O−Si structure (Bertoluzza et al., 1982; Jabbour et al., 2008). With increasing temperature, the peak width at 1050 cm^{-1} increases and the peak intensity at 773 cm^{-1} and 450 cm^{-1} increases, revealing that the three-dimensional network structure of Si−O−Si is gradually formed and reinforced during sintering. The peak at 1466 cm^{-1} is related to CO_3^{2-} (Chen
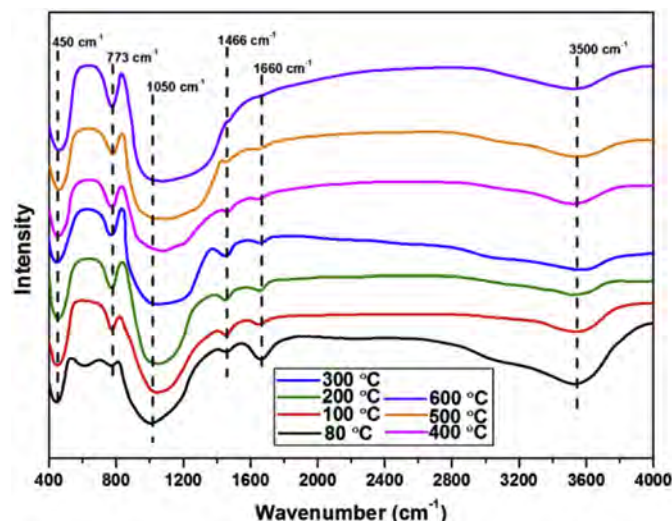
et al., 2009; Li et al., 2015). The intensity increases from 80 to 200 °C and then decreases significantly as the temperature continues to rise because the amount of Na_2CO_3 formed by the reaction between water glass and CO_2 in air increases as the temperature rises from 80 to 200 °C and also because Na_2CO_3 is gradually decomposed when the temperature is above 200 °C. Fig. 7 shows the ^{29}Si MAS NMR spectra of the samples prepared at different temperature. The two-dimensional layered structure of Si-O-Si (Q^3) dominates in the precursor sample at 80 °C. The resonance peak intensity of Q^4 improves as the temperature increases, indicating that the highly polymerized three-dimensional Si-O-Si framework is gradually formed as the temperature goes up. On the micro-level, solidification and molding of the foamed ceramics can be interpreted as a silicate polymerization process in which the two-dimensional Si-O-Si layers spontaneously crosslink to form a three-dimensional Si-O-Si network as the temperature is increased. The ^{29}Si MAS NMR analysis corroborates the FTIR results.

2.3. Characterization of the final products

The properties of the as-obtained porcelain ceramic tiles and foamed ceramic samples are determined as shown in Table 4. The as-obtained porcelain ceramic tile possesses more attractive properties such as the higher flexural strength, greater apparent density, lower water absorption, smaller open porosity, and better thermal shock resistance. The loss on ignition and linear shrinkage of the as-obtained sample are slightly higher than those of the reference sample, and the as-obtained sample has a lighter color as well. The as-obtained porcelain ceramic tile meets the requirements for the Chinese standard for ceramic tiles (GB/T 4100−2015, ISO 13006:2012) and can be used in industrial production and technology. Therefore, using activated CFA as the raw materials improves the properties of the porcelain ceramic tiles. From the micro perspective, the ceramic performance improvement induced by activated CFA can be explained. The SEM images show that there are many needle-shaped crystals (red dashed ellipses) inside the as-obtained porcelain ceramic tile, whereas many unreacted CFA particles (red dashed circles) are observed frm the reference sample, as shown in Fig. 8(a) and (b). According to EDS, the needle-shape crystals are mullite (see Fig. 8(c)). Mullite crystals have excellent mechanical properties and the existence of needle-shaped mullite in the ceramics improve the properties of the final
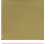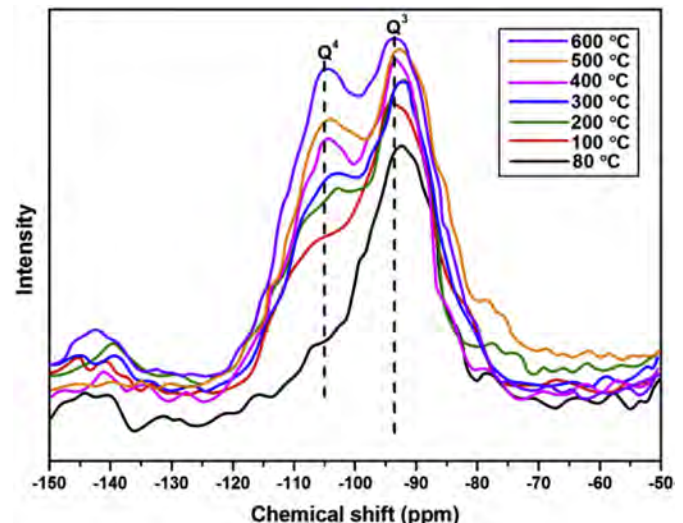

Fig. 6. FTIR spectra of the samples prepared at different temperature.

Fig. 7. ^{29}Si MAS NMR spectra of the samples prepared at different temperature.

Table 4
Optimal properties of the as-obtained porcelain ceramic tile sample and reference sample.

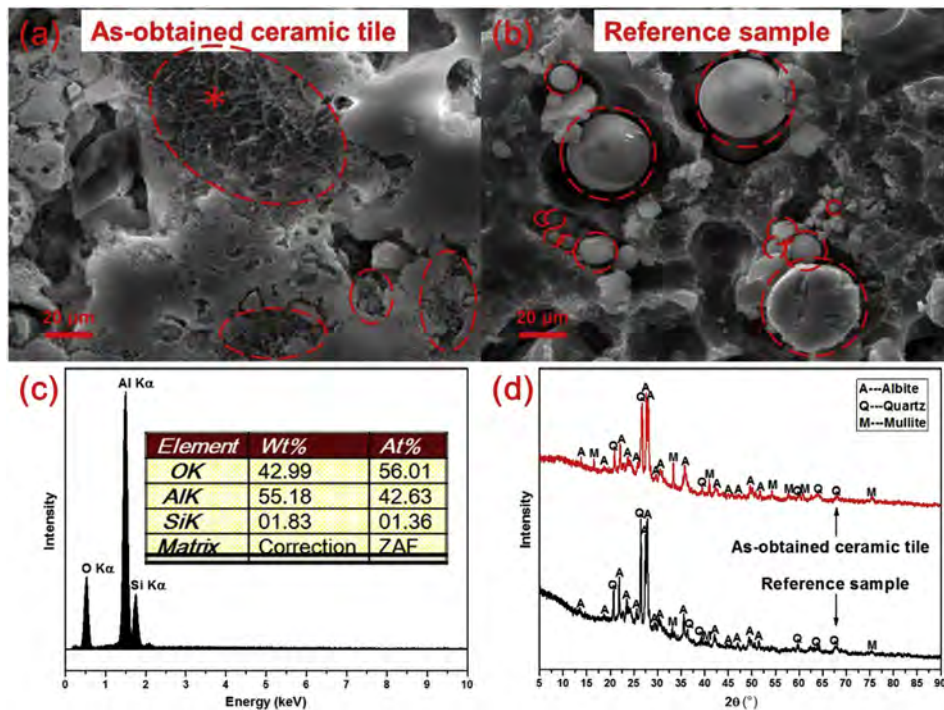| Sample	Flexural strength (MPa)	Apparent density (g/cm³)	Water absorption (%)	Open porosity (%)	Thermal shock resistance (Time)	Loss on ignition (wt %)	Linear shrinkage (%)	Color
As-obtained sample	40.25	2.35	0.30	0.62	11	6.48	14.94	
Reference sample	32.58	2.26	0.50	0.89	5	3.99	11.25	
Standard requirement	≥35	–	≤0.5	–	10	–	–	

Sintering temperature: 1100 °C.

Fig. 8. Characterization of as-obtained porcelain ceramic tile sample and reference sample: (a, b) SEM images, (c) EDS analysis of Fig. 8(a), and (d) XRD patterns.

products (Ke et al., 2016). Therefore, the excellent properties of the as-obtained porcelain ceramic tile can be attributed to the formation of needle-shaped mullite crystals. Combined with the chemical composition of activated CFA in Table 2 and activation mechanism analysis in Section 3.1, it can be inferred that the activated CFA with a mullite composition and highly reactive silicate structure can transform into needle-shape mullite crystals during sintering. The untreated CFA merely serves as an inert filler similar to quartz due to the poor sintering activity. The XRD patterns in Fig. 8(d) confirms that the as-obtained porcelain ceramic tile has a considerable number of mullite crystals but there is very little mullite phase in the reference sample.

The optimal properties of the as-obtained foamed ceramic sample are presented in Table 5. The foamed ceramic sample has a small apparent density of 0.13 g/cm³, high porosity of 94.58%, and low thermal conductivity of 0.0453 W/m·K. The low thermal conductivity indicates that it is an architectural thermal insulation material due to the unique structure. Fig. 9 reveals of cavity construction and zigzag cavity walls can be observed. The thermal processes include conduction, convection and radiation (Dehghan et al., 2015). This unique cavity structure contains air which blocks thermal conduction and the zigzag cavity walls impede thermal convection and radiation. Therefore, the sample has low

Table 5
Optimal properties of the as-obtained foamed ceramic sample.

Apparent density (g/cm³)	Porosity (%)	Thermal conductivity (W/m·K)	Compressive strength (MPa)
0.13	94.58	0.0453	0.77

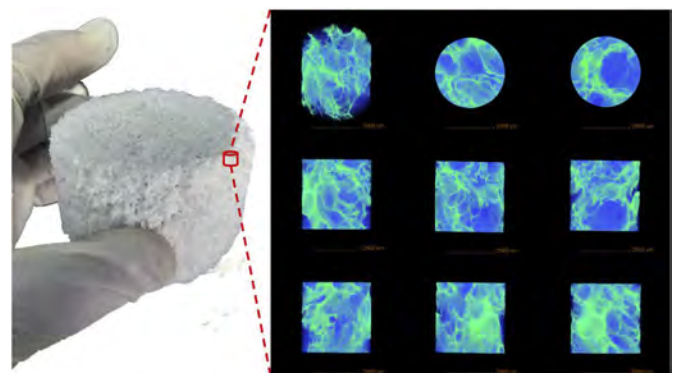Sintering temperature: 600 °C.

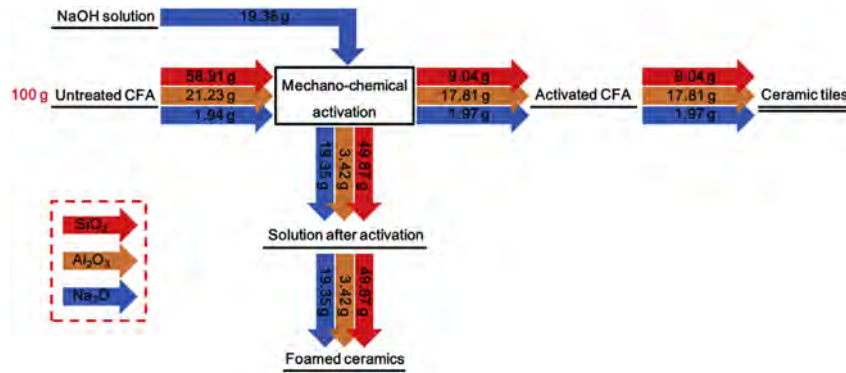**Fig. 9.** Macro and micro morphologies of the as-obtained foamed ceramic sample.

Fig. 10. Substance flow diagram of Al_2O_3, SiO_2 and Na_2O.

thermal conductivity. In addition, the relatively uniform cavity size provides high compressive strength since the external load is uniformly distributed in the cavity walls of the porous structure. Finally, by examining the 3D image of the foamed sample on the right in Fig. 9, the micro morphology of the cavity structure is similar to the boiling morphology of the liquid. Therefore, it can be deduced that the cavity structure results from the water-vaporization-induced vacancies and the morphology is preserved by silicate solidification during sintering.

2.4. Process cleanliness consideration

The substance flow, gas emission, and heavy metal leaching are investigated. The substance flow analysis is carried out first. The main components of CFA are SiO_2 and Al_2O_3, which together account for more than 80 wt% and the activator in this study is the NaOH solution. Hence, the substance flows of Al_2O_3, Si_2O and Na_2O in the whole process are analyzed (see Fig. 10) using 100 g of CFA. In mechanochemical activation, most of the SiO_2 in the CFA (84.65%) enters the solution, while the majority of Al_2O_3 remains in the solid phase (83.89%). Although Na_2O is mainly retained in the solution, a small part (0.15%) enters the structure of the activated CFA. From the view of the chemical component, it can be concluded that the excess SiO_2 in CFA leaches into the alkaline solution and so the chemical composition of CFA is adjusted to be closer to that of mullite. At the same time, a high-modulus sodium silicoaluminate solution can be obtained and used as the proper raw materials for the new foamed ceramics.

Gas emission is one of the important environmental requirements in the sintering process (Li et al., 2018b). In this study, gas emission mainly results from heating of the solution after activation. Together with the TG-DSC analysis in Section 3.2, it can

be inferred that the emitted gas is mainly H_2O vapor which does not pollute the environment. Table 4 shows that the loss on ignition of as-obtained porcelain ceramic samples is small (6.48 wt%), indicating a very small amount of gas emission (including CO_2 derived from carbon in CFA and H_2O vapor from the raw materials) during sintering of the porcelain ceramic tiles. Hence, the environmental impact is negligible.

Finally, the heavy metal leaching behavior is evaluated. Table 6 shows the heavy metal contents in CFA and Table 7 shows the heavy metal leaching results of the final products based on GB 5086.2–1997. The amounts of nine heavy metals leached are well below the Chinese leaching toxicity identification standard values stipulated in GB 5085.3–2007. The leaching amounts of heavy metals from the porcelain tiles are obviously less than those from the foamed ceramics resulting from the better heavy metal encapsulation during higher temperature sintering. In short, the final ceramic products are safe to human health and environment.

There is almost no hazardous waste emission in the CFA treatment process and ceramic manufacturers can produce two new types of ceramic products simultaneously. Therefore, this process is eco-friendly and cleaner for CFA utilization for ceramics production.

3. Conclusion

An eco-friendly and cleaner process for preparing architectural ceramics from CFA is described. During mechanochemical activation of CFA, 28.05% of Al (VI) is converted into Al (IV) which can substitute for Si^{4+} in the tetrahedral rendering the silicate structure of activated CFA more unstable than the untreated CFA. The silicate network structure gradually depolymerizes during activation and Na ions are adsorbed or bound to the structure of activated CFA to balance the charge deficit from replacement of Si^{4+} by Al^{3+}. The activated CFA is used as raw materials to prepare porcelain ceramic tiles and the solution is used to prepare foamed thermal insulation ceramics. The activated CFA with a mullite-like composition and highly reactive silicate structure transforms into needle-shaped mullite crystals during sintering, thereby significantly contributing to the mechanical properties of porcelain ceramic tiles. The low thermal conductivity of 0.0453 W/m·K of the as-obtained

Table 6
Contents of heavy metals in CFA (µg/g) measured by ICP-MS.

Heavy metal	Hg	Pb	Cd	Cr	Cu	Zn	Ba	Ni	As
Content	0.8	37.1	0.8	313.4	70.6	145.2	799.0	152.6	91.7

Table 7
Leaching test results for the obtained porcelain ceramic tiles and foamed ceramics (µg/L) measured by ICP-MS.

Sample	Hg	Pb	Cd	Cr	Cu	Zn	Ba	Ni	As
Porcelain tile	0.2	0.1	0.0	5.4	1.9	3.3	4.1	0.1	6.9
Foamed ceramic	7.1	27.4	0.8	11.3	8.6	9.1	31.9	1.2	10.1
Standard limit (GB 5085.3–2007)	50	3000	300	10000	50000	50000	100000	10000	1500

Note: GB 5085.3–2007 is matched with the operation standard of GB 5086.2–1997.

foamed ceramic sample is attributed to the unique cavity construction. On the micro level, solidification of foamed ceramics can be interpreted as the Si-O-Si structure transforming from two-dimensional layers into a three-dimensional network during sintering. Analyses of the substance flow, gas emission, and heavy metal leaching of the final products indicate that the materials are eco-friendly and safe. However, more varieties of CFAs are necessary to clearly verify the universality of this technique. In addition, future research on this process should consider the sustainability and cost in more details as well as energy related issues. This study should help to solve the problem related to CFA storage and ceramic raw materials shortage in China and the technique is feasible industrially.

4. Declarations of interest

None.

Acknowledgments

Appendix A. Supplementary data

Supplementary data to this article can be found online at https://doi.org/10.1016/j.jclepro.2018.12.292.

References

Allouhi, A., El Fouih, Y., Kousksou, T., Jamil, A., Zeraouli, Y., Mourad, Y., 2015. Energy consumption and efficiency in buildings: current status and future trends. J. Clean. Prod. 109, 118–130.

Bertoluzza, A., Fagnano, C., Morelli, M.A., Gottardi, V., Guglielmi, M., 1982. Raman and infrared spectra on silica gel evolving toward glass. J. Non-Cryst. Solids 48, 117–128.

Bontempi, E., 2017. A new approach for evaluating the sustainability of raw materials substitution based on embodied energy and the CO_2 footprint. J. Clean. Prod. 162, 162–169.

Cao, W., Cheng, X., Gong, L., Li, Y., Zhang, R., Zhang, H., 2015. Thermal conductivity of highly porous ceramic foams with different agar concentrations. Mater. Lett. 139, 66–69.

Carty, W.M., Senapati, U., 1998. Porcelain—raw materials, processing, phase evolution, and mechanical behavior. J. Am. Ceram. Soc. 81, 3–20.

Chen, Y., Hong, Y., Zheng, F., Li, J., Wu, Y., Li, L., 2009. Preparation of silicate stalagmite from sodium silicate. J. Alloy. Comp. 478, 411–414.

Dana, K., Das, S., Das, S.K., 2004. Effect of substitution of fly ash for quartz in triaxial kaolin—quartz—feldspar system. J. Eur. Ceram. Soc. 24, 3169–3175.

Das, S.K., Pal, M., Ghosh, J., Pathi, K.V., Mondal, S., 2013. The effect of basic oxygen furnace slag and fly ash additions in triaxial porcelain composition: phase and micro structural evolution. T. Indian. I. Metals. 66, 213–220.

Dědeček, J., Sklenak, S., Li, C., Gao, F., Brus, J., Zhu, Q., Tatsumi, T., 2009. Effect of Al/Si substitutions and silanol nests on the local geometry of Si and Al framework sites in silicone-rich zeolites: a combined high resolution ^{27}Al and ^{29}Si NMR and density functional theory/molecular mechanics study. J. Phys. Chem. C 113, 14454–14466.

Dehghan, M., Mahmoudi, Y., Valipour, M.S., Saedodin, S., 2015. Combined conduction—convection—radiation heat transfer of slip flow inside a micro-channel filled with a porous material. Transport Porous Media 108, 413–436.

Fernández-Jiménez, A., De La Torre, A.G., Palomo, A., López-Olmo, G., Alonso, M.M., Aranda, M.A.G., 2006. Quantitative determination of phases in the alkali activation of fly ash. Part I. Potential ash reactivity. Fuel 85, 625–634.

Gao, X., Yu, Q.L., Brouwers, H.J.H., 2017. Apply ^{29}Si, ^{27}Al MAS NMR and selective dissolution in identifying the reaction degree of alkali activated slag-fly ash composites. Ceram. Int. 43, 12408–12419.

Han, L., Li, F., Deng, X., Wang, J., Zhang, H., Zhang, S., 2017. Foam-gelcasting preparation, microstructure and thermal insulation performance of porous diatomite ceramics with hierarchical pore structures. J. Eur. Ceram. Soc. 37, 2717–2725.

He, H., Guo, J., Zhu, J., Yuan, P., Hu, C., 2004. 29Si and 27Al MAS NMR spectra of mullites from different kaolinites. Spectrochim. Acta A. 60, 1061–1064.

Huang, Y., Luo, J., Xia, B., 2013. Application of cleaner production as an important sustainable strategy in the ceramic tile plant—a case study in Guangzhou, China. J. Clean. Prod. 43, 113–121.

Jabbour, J., Calas, S., Gatti, S., Kribich, R.K., Myara, M., Pille, G., Etienne, P., Moreau, Y., 2008. Characterization by IR spectroscopy of an hybrid sol—gel material used for photonic devices fabrication. J. Non-Cryst. Solids 354, 651–658.

Kairytė, A., Kirpluks, M., Ivdre, A., Cabulis, U., Vaitkus, S., Pundienė, I., 2018. Cleaner production of polyurethane foam: replacement of conventional raw materials, assessment of fire resistance and environmental impact. J. Clean. Prod. 183, 760–771.

Kamseu, E., Leonelli, C., Boccaccini, D.N., Veronesi, P., Miselli, P., Pellacani, G., Melo, U.C., 2007. Characterisation of porcelain compositions using two China clays from Cameroon. Ceram. Int. 33, 851–857.

Ke, S., Wang, Y., Pan, Z., Ning, C., Zheng, S., 2016. Recycling of polished tile waste as a main raw material in porcelain tiles. J. Clean. Prod. 115, 238–244.

Klinowski, J., Thomas, J.M., Fyfe, C.A., Gobbi, G.C., Hartman, J.S., 1983. A highly siliceous structural analog of zeolite Y: high-resolution solid-state silicon-29 and aluminum-27 NMR studies. Inorg. Chem. 22, 63–66.

Kockal, N.U., 2012. Utilisation of different types of coal fly ash in the production of ceramic tiles. Bol. Soc. Esp. Ceram. V. 51, 297–304.

König, J., Petersen, R.R., Yue, Y., 2015. Fabrication of highly insulating foam glass made from CRT panel glass. Ceram. Int. 41, 9793–9800.

Kumar, S., Singh, K.K., Ramachandrarao, P., 2001. Effects of fly ash additions on the mechanical and other properties of porcelainised stoneware tiles. J. Mater. Sci. 36, 5917–5922.

Leonelli, C., Bondioli, F., Veronesi, P., Romagnoli, M., Manfredini, T., Pellacani, G.C., Cannillo, V., 2001. Enhancing the mechanical properties of porcelain stoneware tiles: a microstructural approach. J. Eur. Ceram. Soc. 21, 785–793.

Li, D., Wu, D., Xu, F., Lai, J., Shao, L., 2018. Literature overview of Chinese research in the field of better coal utilization. J. Clean. Prod. 185, 959–980.

Li, J., Zhuang, X., Monfort, E., Querol, X., Llaudis, A.S., Font, O., Izquierdo, M., 2018. Utilization of coal fly ash from a Chinese power plant for manufacturing highly insulating foam glass: implications of physical, mechanical properties and environmental features. Constr. Build. Mater. 175, 64–76.

Liu, X., Zhang, N., Yao, Y., Sun, H., Feng, H., 2013. Micro-structural characterization of the hydration products of bauxite-calcination-method red mud-coal gangue based cementitious materials. J. Hazard Mater. 262, 428–438.

Li, Y., Cheng, X., Cao, W., Gong, L., Zhang, R., Zhang, H., 2015. Fabrication of adiabatic foam at low temperature with sodium silicate as raw material. Mater. Des. 88, 1008–1014.

Loewenstein, W., 1954. The distribution of aluminum in the tetrahedra of silicates and aluminates. Am. Mineral. 39, 92–96.

Luo, Y., Zheng, S., Ma, S., Liu, C., Wang, X., 2017. Ceramic tiles derived from coal fly ash: preparation and mechanical characterization. Ceram. Int. 43, 11953–11966.

Luo, Y., Zheng, S., Ma, S., Liu, C., Wang, X., 2018. Preparation of sintered foamed ceramics derived entirely from coal fly ash. Constr. Build. Mater. 163, 529–538.

Ma, Z., Tian, X., Liao, H., Guo, Y., Cheng, F., 2018. Improvement of fly ash fusion characteristics by adding metallurgical slag at high temperature for production of continuous fiber. J. Clean. Prod. 171, 464–481.

Mukhopadhyay, T.K., Ghosh, S., Ghosh, J., Ghatak, S., Maiti, H.S., 2010. Effect of fly ash on the physico-chemical and mechanical properties of a porcelain composition. Ceram. Int. 36, 1055–1062.

Novais, R.M., Buruberri, L.H., Ascensão, G., Seabra, M.P., Labrincha, J.A., 2016. Porous biomass fly ash-based geopolymers with tailored thermal conductivity. J. Clean. Prod. 119, 99–107.

Oh, J.E., Jun, Y., Jeong, Y., 2014. Characterization of geopolymers from compositionally and physically different Class F fly ashes. Cement Concr. Compos. 50, 16–26.

Oh, J.E., Jun, Y., Jeong, Y., Monteiro, P.J., 2015. The importance of the network-modifying element content in fly ash as a simple measure to predict its strength potential for alkali-activation. Cement Concr. Compos. 57, 44–54.

Olgun, A., Erdogan, Y., Ayhan, Y., Zeybek, B., 2005. Development of ceramic tiles from coal fly ash and tincal ore waste. Ceram. Int. 31, 153–158.

Pal, M., Das, S.K., 2018. Phase and microstructural evolution in quartz-free porcelain tile compositions. J. Australas. Ceram. Soc. 54, 109–117.

Park, J.H., Edraki, M., Mulligan, D., Jang, H.S., 2014. The application of coal combustion by-products in mine site rehabilitation. J. Clean. Prod. 84, 761–772.

Rao, A.P., Rao, A.V., Pajonk, G.M., 2007. Hydrophobic and physical properties of the ambient pressure dried silica aerogels with sodium silicate precursor using various surface modification agents. Appl. Surf. Sci. 253, 6032–6040.

Reinosa, J.J., Del Campo, A., Fernández, J.F., 2015. Indirect measurement of stress distribution in quartz particles embedded in a glass matrix by using confocal Raman microscopy. Ceram. Int. 41, 13598–13606.

Shi, J., Liu, H., Lou, Z., Zhang, Y., Meng, Y., Zeng, Q., Yang, M., 2013. Effect of interlayer counterions on the structures of dry montmorillonites with Si^{4+}/Al^{3+} substitution. Comput. Mater. Sci. 69, 95–99.

Sun, G.K., Young, J.F., Kirkpatrick, R.J., 2006. The role of Al in C–S–H: NMR, XRD, and compositional results for precipitated samples. Cement Concr. Res. 36, 18–29.

Sun, L.Y., Luo, K., Fan, J.R., Lu, H.L., 2017. Experimental study of extracting alumina from coal fly ash using fluidized beds at high temperature. Fuel 199, 22–27.

Turkmen, O., Kucuk, A., Akpinar, S., 2015. Effect of wollastonite addition on sintering of hard porcelain. Ceram. Int. 41, 5505–5512.

Wattanasiriwech, D., Wattanasiriwech, S., 2011. Fluxing action of illite and microcline in a triaxial porcelain body. J. Eur. Ceram. Soc. 31, 1371–1376.

Wang, H., Chen, Z., Liu, L., Ji, R., Wang, X., 2018. Synthesis of a foam ceramic based on ceramic tile polishing waste using SiC as foaming agent. Ceram. Int. 44, 10078–10086.

Wang, J., Qin, Q., Hu, S., Wu, K., 2016. A concrete material with waste coal gangue

and fly ash used for farmland drainage in high groundwater level areas. J. Clean. Prod. 112, 631–638.

Wons, W., Rzepa, K., Reben, M., Murzyn, P., Sitarz, M., Olejniczak, Z., 2018. Effect of thermal processing on the structural characteristics of fly ashes. J. Mol. Struct. 1165, 299–304.

Yao, Z.T., Ji, X.S., Sarker, P.K., Tang, J.H., Ge, L.Q., Xia, M.S., Xi, Y.Q., 2015. A comprehensive review on the applications of coal fly ash. Earth Sci. Rev. 141, 105–121.

Zheng, K., Zhang, Z., Yang, F., Sridhar, S., 2012. Molecular dynamics study of the structural properties of calcium aluminosilicate slags with varying Al_2O_3/SiO_2 ratios. ISIJ Int. 52, 342–349.

Zhu, M., Ji, R., Li, Z., Wang, H., Liu, L., Zhang, Z., 2016. Preparation of glass ceramic foams for thermal insulation applications from coal fly ash and waste glass. Constr. Build. Mater. 112, 398–405.

Supplementary Material

1. Influence of peak temperature on the properties of sintered porcelain ceramic tiles

Table S1 Properties of the porcelain ceramic tiles sintered at different peak temperatures.

Sample	Flexural strength (MPa)	Apparent density (g/cm^3)	Water absorption (%)	Open porosity (%)	Thermal shock resistance (Time)	Linear shrinkage (%)	Color
1000 °C	30.39	1.84	14.50	23.55	5	6.24	
1050 °C	35.88	2.19	4.45	10.85	13	11.78	
1100 °C	40.25	2.35	0.30	0.62	11	14.94	
1150 °C	30.78	2.39	0.00	0.00	8	15.99	

Residence time = 1 h.

2. Influence of residence time on the properties of sintered porcelain ceramic tiles

Table S2 Properties of the porcelain ceramic tiles sintered at different residence time.
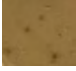
Sample	Flexural strength (MPa)	Apparent density (g/cm^3)	Water absorption (%)	Open porosity (%)	Thermal shock resistance (Time)	Linear shrinkage (%)	Color
20 min	16.96	1.80	17.34	30.17	4	4.99	
40 min	31.06	2.12	7.36	13.79	8	10.83	

60 min	40.25	2.35	0.30	0.62	11	14.94	
80 min	37.64	2.37	0.00	0.00	10	15.41	

Peak temperatures = 1100 °C.

3. Pre-digestion method for solid samples before the ICP-OES analysis

To determine the contents of Al_2O_3, SiO_2, Fe_2O_3, TiO_2, CaO, and MgO, a kind of alkaline fusion and acid leaching of the solid residue using ICP-OES was established (Todand et al., 1995). The mixture of Na_2CO_3 and $Na_2B_4O_7 \cdot 10H_2O$ in the mass ratio of 2:1 was used as the molten solvent. A certain amount of the solid residue was mixed with the molten solvent and then the sample was calcined in muffle furnace at 950℃ for 15min. After sintering of high temperature, the major elements, such as Al. Si, Fe, Ti, Ca, Mg were all converted into sodium salts. At last, the sintering products then react with diluted hydrochloric acid solution. After the acid leaching, the solution was diluted with water to 100mL. We can calculate the compositions of the solid residue by measuring the contents of the final solution using ICP-OES. As for Na_2O and K_2O measurement, a similar pretreatment method without alkaline fusion step was adopted. After the diluted hydrochloric acid leaching, Na and K elements were totally dissolved and can be calculated by measuring the contents of the final solution using ICP-OES.

Reference

Todand, M.M., Jarvis, I., Jarvis, K.E., 1995. Microwave digestion and alkali fusion procedures for the determination of the platinum-group elements and gold in geological materials by ICP-MS. Chem. Geol. 124, 21－36.